Nonequilibrium response of magnetic nanoparticles to time-varying magnetic fields: contributions from Brownian and Néel processes

Article

Accepted Version

It is advisable to refer to the publisher's version if you intend to cite from the work. See Guidance on citing.

To link to this article DOI: http://dx.doi.org/10.1103/PhysRevE.109.034603

www.reading.ac.uk/centaur

Nonequilibrium response of magnetic nanoparticles to time–varying magnetic fields beyond linear response: contributions from Brownian and Néel processes

Patrick Ilg

School of Mathematical, Physical, and Computational Sciences,
University of Reading, Reading, RG6 6AX, United Kingdom

Many technical and biomedical applications of magnetic nanoparticles rely on their response to time–varying magnetic fields. While well–established models exist for either immobile or thermally blocked nanoparticles, the intermediate regime where Brownian as well as Néel relaxation occur at the same time is less well explored. Here, we use an efficient model that allows us to study the non-linear dynamics of individual magnetic nanoparticles in response to different time–varying magnetic fields over a broad range of field parameters, taking into account both relaxation mechanisms. We provide quasi–exact solutions for the longitudinal dynamics as well as approximate formulae from dynamic mean–field theory. Our results are relevant e.g. for magnetorelaxometry, magnetic fluid hyperthermia and magnetic particle imaging. For these example applications, we show that the ratio of characteristic Brownian to Néel relaxation time can have a profound impact on characteristic response quantities, especially at large field strengths.

I. INTRODUCTION

Colloidal magnetic nanoparticles (MNPs) suspended in viscous carrier media are known as ferrofluids and have attracted considerable attention as field–responsive materials since their properties can be manipulated by external fields [56]. In recent years, several exciting technical and biomedical applications of MNPs have been explored [57–59]. Within these biomedical applications, the response of MNPs to time–varying magnetic fields is of crucial importance [60]. In magnetorelaxometry, for example, a step–change in the magnetic field is used to detect the binding kinetics of coated MNPs [61, 62]. When large molecules bind to the surface and hinder the rotational motion of the MNPs, the resulting changes in the magnetization relaxation can be detected, which allows to determine the amount and time of binding. Another example is Magnetic Fluid Hyperthermia (MFH), which is a promising tumor therapy where MNPs are used to locally heat tissue with the help of an externally applied oscillating field [63–66]. The magnetic losses within the MNPs – that are created by the magnetization dynamics in response to the oscillating magnetic field – are transferred to heat which is then released to the neighborhood of the nanoparticle. In magnetic particle imaging (MPI), on the other hand, the response of tracer MNPs to static and oscillating fields is used to obtain high-resolution images [67–70].

Significant efforts have been undertaken to bring these promising methods into clinical applications [59, 64, 70, 71]. Thereby, one focus has been to improve the efficiency of the methods and at the same time to reduce possible side effects. Several studies have addressed the synthesis and choice of the most suitable MNPs for the specific applications [72, 73] as well as finding the corresponding optimal magnetic fields [74, 75]. However, finding optimal conditions is a very demanding task since the parameter space is very large. Therefore, overly simplified model assumptions are often made to design and inter-

pret MNP applications [64]. Typically, non–interacting MNPs with equilibrium, field–independent properties are assumed that are either governed solely by Brownian or solely by Néel relaxation. The latter assumption is particularly problematic since these processes show very different field dependencies, such that seemingly irrelevant processes at zero field can become dominant at strong fields [76, 77]. A recent review of theoretical approaches [78] concludes that equilibrium and linear models are typically insufficient to model the nonequilibrium dynamics in the nonlinear regime that arises in MFH and MPI.

To account for the nonlinear dynamics of the coupled field–dependent Brownian and Néel relaxation, the so–called "egg model" combines the stochastic Landau–Lifshitz–Gilbert (LLG) equation of the internal magnetization dynamics with the rotational Brownian particle motion in a viscous medium [79, 80]. This model has been used e.g. to study hysteresis curves [81] and response to oscillating fields [82], as well as mode–coupling effects and non–exponential relaxation [77]. However, despite some recent advances [83, 84], the egg model remains computationally very demanding for magnetically hard MNPs with large anisotropy barriers. In this case, there is a huge gap in time scales between the microscopic attempt frequency and the effective Néel relaxation time resulting from rare, thermally activated magnetization reversals.

Here, instead, we use an efficient diffusion–jump (DJ) model for magnetically hard MNPs [85] that is able to describe the coupled nonequilibrium dynamics of field–induced Brownian and Néel relaxation in the fully non-linear regime. We here focus on the ultra–dilute regime and consider only non–interacting MNPs. For interaction and concentration effects see e.g. Refs. [86–88] and references therein. Besides approximate analytical expressions that are useful to discuss various trends, we also provide quasi–exact solutions to the DJ model. Quasi–exact solutions are obtained by transforming the original model formulation into a system of linear ordinary differential equations that can be solved with great accuracy.

We illustrate the model and investigate its predictions for several cases of interest for biomedical applications. The paper is organized as follows. First, the model is introduced in Sec. II. Then, solutions to the model are discussed in Sec. III. First, approximations to the model are derived in Sec. III A before quasi–exact solutions are found for the longitudinal dynamics by expansion into Legendre polynomials in Sec. III B. Results and predictions of the model are presented in Sec. IV. First, the spectrum of relaxation times and their weights are given in Sec. IV A. Furthermore, we consider the magnetization response to a step–change in the magnetic field in Sec. IV B, similar to the situation in MRX. The field–dependent AC susceptibility is investigated in Sec. IV C before the response to an oscillating field for a range of amplitudes is discussed in Sec. IV D with an eye on MFH applications. Lastly, the tracer response to a high frequency oscillating field superposed to a static bias field as in MPI is studied in Sec. IV E. Finally, we discuss the proposed model and approach in Sec. V and set it into the wider context before conclusions are offered in Sec. VI.

II. DIFFUSION–JUMP MODEL

A. Justifications and limitations of the model

The stochastic LLG equation and its extension to the egg model are well established models to describe the dynamics of frozen and mobile magnetic nanoparticles, respectively [79, 80]. The stochastic LLG equation describes the dynamics of the magnetization and the particle's easy axis on the timescale of the attempt frequency, typically on the order of $\tau_0 \sim 10^{-10} \ldots 10^{-9}$s [56]. The Néel relaxation time τ_N describes magnetization reversals over the magnetic anisotropy barrier and grows exponentially with the magnetic volume of the nanoparticle [56, 89]. For many MNPs used in technical and medical applications a time-scale separation is found, $\tau_N \gg \tau_0$, and the LLG and egg model become extremely inefficient to describe the long-time/low-frequency dynamics [86]. For spatially frozen MNPs, several authors have therefore replaced the LLG equation with an empirical kinetic Monte-Carlo scheme to model magnetization reversals on time scales large compared to τ_0 [90–93]. Such approaches can be interpreted as the result of integrating out the fast vibrations of the magnetization around the easy axis of the MNP. For mobile MNPs, the situation is more complicated as a third time scale (τ_B) appears which characterizes the rotational Brownian diffusion of the nanoparticle. Since $\tau_B \gg \tau_0$ for typical MNPs, an approach combining rotational particle diffusion with kinetic Monte-Carlo methods representing magnetization reversals has been suggested [85, 86, 94]. Eliminating the microscopic time scale τ_0, the diffusion-jump (DJ) model [85] is not only very efficient, but has also been shown to give quantitatively accurate results compared to the un-

derlying egg model for large magnetic anisotropies with $\tau_N \gg \tau_0$ and not too high frequencies $\omega \ll 1/\tau_0$ [77]. Thus, in a sense, the DJ model can be considered as correction to the rigid-dipole approximation for mobile and magnetically hard MNPs.

B. Model formulation

Starting point is the diffusion–jump equation [85] for the time-dependent single–particle probability density function (pdf) $f(\mathbf{u}; t)$ for the orientation $\mathbf{u}$ of the magnetic moment at time t,

$$\frac{\partial}{\partial t} f(\mathbf{u}; t) = [\mathrm{L_B}(\mathbf{h}) + \mathrm{L_N}(\mathbf{h})] f(\mathbf{u}; t). \qquad (1)$$

As mentioned in Sec. II A, we assume sufficiently large magnetic anisotropy barriers that the magnetic moment can be considered to be well-aligned with the easy axis of the MNP. From the solution $f(\mathbf{u}; t)$ to Eq. (1), we can calculate all quantities of interest as the time–dependent expectation values of $\mathbf{u}$. The dimensionless magnetization at time t, for example, is obtained by

$$\mathbf{m}(t) = \int \mathbf{u} f(\mathbf{u}; t) \mathrm{d}\mathbf{u}, \qquad (2)$$

where the integration is performed over the three–dimensional unit sphere. In Eq. (1), the Brownian rotational diffusion (Fokker–Planck) part is identical to the classical model proposed by Martsenyuk *et al.* [95],

$$\mathrm{L_B}(\mathbf{h}) f = \frac{1}{2\tau_B} \left[\boldsymbol{\mathcal{L}}^2 f - \boldsymbol{\mathcal{L}} \cdot f \boldsymbol{\mathcal{L}}(\mathbf{u} \cdot \mathbf{h}) \right], \qquad (3)$$

where τ_B denotes the Brownian rotational diffusion time of a single MNP in a viscous medium and $\boldsymbol{\mathcal{L}} = \mathbf{u} \times \partial/\partial \mathbf{u}$ the rotational operator. The action of an external magnetic field $\mathbf{H}$ is described by the dimensionless field $\mathbf{h} = \mu_0 \mu \mathbf{H}/k_B T$ with $h = |\mathbf{h}|$ its magnitude, μ_0 the permeability of free space, μ the magnetic moment of the MNP, and $k_B T$ the thermal energy. Note that an explicit time–dependence enters the operator only via the external field $\mathbf{H}$ which might be time–dependent, $\mathrm{L_B}(\mathbf{h}(t))$.

Without the contribution $\mathrm{L_N}(\mathbf{h})$, the model (1) corresponds to the rigid–dipole approximation where MNPs are considered to be thermally blocked such that Néel relaxation can be ignored. Properties of the model in the rigid–dipole approximation have been studied quite extensively [96–99]. The DJ model [85] goes beyond the rigid–dipole approximation and includes Néel relaxation in the form of jump processes that are described by

$$\mathrm{L_N}(\mathbf{h}) f(\mathbf{u}; t) = \frac{1}{2\tau_N} \left[e^{\mathbf{u} \cdot \mathbf{h}} f(-\mathbf{u}; t) - e^{-\mathbf{u} \cdot \mathbf{h}} f(\mathbf{u}; t) \right], \quad (4)$$

where τ_N denotes the Néel relaxation time. Also for the Néel contribution, explicit time–dependence enters only via the external magnetic field, $\mathrm{L_N}(\mathbf{h}(t))$.

By construction, the DJ model conserves the normalization of the probability density, $\int f(\mathbf{u};t)\mathrm{d}\mathbf{u} = 1$ for any time t. In addition, the Boltzmann equilibrium

$$f_{\mathrm{eq}}(\mathbf{u}) = z_{\mathrm{eq}}^{-1} \exp\left[\mathbf{u} \cdot \mathbf{h}\right] \tag{5}$$

with $z_{\mathrm{eq}} = 4\pi \sinh(h)/h$ is the stationary solution to Eq. (1) for time–independent fields $\mathbf{h}$.

In the absence of external magnetic fields, the DJ model is fully characterized by the bare Brownian (τ_{B}) and bare Néel (τ_{N}) relaxation times and the combined dynamics is governed by the effective relaxation time τ_{eff} defined by [66]

$$\frac{1}{\tau_{\mathrm{eff}}} = \frac{1}{\tau_{\mathrm{B}}} + \frac{1}{\tau_{\mathrm{N}}} \qquad (h = 0). \tag{6}$$

In the results shown below, we typically use τ_{eff} as reference time scale and indicate with $q = \tau_{\mathrm{B}}/\tau_{\mathrm{N}}$ the ratio of these two basic time scales.

III. SOLUTION METHODS

We are primarily interested in the nonequilibrium magnetization dynamics. Taking the time derivative on both sides of Eq. (2) and inserting the kinetic equation (1) leads to [77, 85]

$$\frac{\mathrm{d}}{\mathrm{d}t}\mathbf{m} = -\frac{1}{\tau_{\mathrm{B}}}\mathbf{m} + \frac{1}{2\tau_{\mathrm{B}}}[\mathbf{h} - \langle\mathbf{u}\mathbf{u}\rangle \cdot \mathbf{h}] - \frac{1}{\tau_{\mathrm{N}}}\langle\mathbf{u}\, e^{-\mathbf{u}\cdot\mathbf{h}}\rangle, \tag{7}$$

where we introduced the short notation $\langle\bullet\rangle = \int \bullet f(\mathbf{u};t)\mathrm{d}\mathbf{u}$ for time–dependent averages with respect to $f(\mathbf{u};t)$. As is common in nonequilibrium statistical physics [100], Eq. (7) does not provide a closed time evolution equation for the magnetization since it couples to higher order moments of f. Sections III A and III B present approximate and exact solutions to this equation, respectively.

A. Effective field approximation

A powerful closure approximation within the rigid–dipole limit ($\tau_{\mathrm{N}} \to \infty$) was suggested in [95] and found to be rather accurate for rigid dipoles [101, 102]. Here, we apply this effective field approximation (EFA) to the DJ model. In [77], we instead used a first order perturbation theory for small deviations from equilibrium. EFA is a stronger assumption that allows us to go beyond the linear regime.

To close the magnetization equation, Martsenyuk *et al* [95] suggested to evaluate all expectation values with the following ansatz for the pdf

$$f_{\boldsymbol{\xi}_{\mathrm{e}}}(\mathbf{u}) = \frac{\xi_{\mathrm{e}}}{4\pi \sinh(\xi_{\mathrm{e}})} e^{\xi_{\mathrm{e}}\mathbf{u}\cdot\mathbf{n}}, \tag{8}$$

which is of the same form as the equilibrium pdf (5) but with the applied field $\mathbf{h}$ replaced by an effective field

$\boldsymbol{\xi}_{\mathrm{e}} = \xi_{\mathrm{e}}\mathbf{n}$, where the unit vector $\mathbf{n}$ denotes the orientation of the effective field. Thus, the time–dependent pdf is approximated Eq. (8) with a time–dependent effective field, $f(\mathbf{u};t) \approx f_{\boldsymbol{\xi}_{\mathrm{e}}(t)}(\mathbf{u})$. In equilibrium the effective field reduces to the applied field, $\xi_{\mathrm{e}} = h$ and $\mathbf{n} = \hat{\mathbf{h}}$.

With the ansatz (8), we can evaluate all expressions on the right hand side of the magnetization equation (7) to obtain

$$\frac{\mathrm{d}}{\mathrm{d}t}\mathbf{m} = -\frac{1}{\tau_{\mathrm{B}}}\left[S_1\mathbf{n} - \frac{2+S_2}{6}\mathbf{h} + \frac{S_2}{2}(\mathbf{h}\cdot\mathbf{n})\mathbf{n}\right] - \frac{1}{\tau_{\mathrm{N}}}\frac{\xi_{\mathrm{e}}\sinh(\nu)L(\nu)}{\sinh(\xi_{\mathrm{e}})\nu^2}\boldsymbol{\nu}, \tag{9}$$

where $\mathbf{m} = S_1\mathbf{n}$ and $S_k = \langle P_k(\mathbf{u}\cdot\mathbf{n})\rangle$ denote the orientational order parameters with $P_k(x)$ the kth order Legendre polynomial. Evaluating the averages with the help of (8) we find $S_k = L_k(\xi_{\mathrm{e}})$ with

$$L_k(x) = \frac{I_{k+1/2}(x)}{I_{1/2}(x)}, \tag{10}$$

where $I_n(x)$ denote modified Bessel functions [97]. Note that $L_1(x)$ equals the Langevin function $L(x) = \coth(x) - 1/x$. In Eq. (9) we have also introduced the deviation of the effective field from the applied field, $\boldsymbol{\nu} = \boldsymbol{\xi}_{\mathrm{e}} - \mathbf{h}$, and its magnitude $\nu = |\boldsymbol{\nu}|$.

The ansatz (8) solves the closure problem in Eq. (7) since the approximate magnetization equation (9) depends only on the effective field $\boldsymbol{\xi}_{\mathrm{e}}$. For practical purposes, it is more convenient to solve for the time–dependent effective field $\boldsymbol{\xi}_{\mathrm{e}}(t)$ first and calculate the resulting magnetization from $\mathbf{m} = S_1\mathbf{n}$ with $S_1(t) = L_1(\xi_{\mathrm{e}}(t))$ [102]. To derive the time evolution equations for the effective field, we use $\dot{\mathbf{m}} = \dot{S}_1\mathbf{n} + S_1\dot{\mathbf{n}}$ with $\dot{S}_1 = L'(\xi_{\mathrm{e}})\dot{\xi}_{\mathrm{e}}$, where the dot is a short notation for the time derivative and $L'(x) = \mathrm{d}L(x)/\mathrm{d}x$. From scalar multiplication of Eq. (9) with $\mathbf{n}$ and using $\dot{\mathbf{n}} \cdot \mathbf{n} = 0$ we find

$$\frac{\mathrm{d}}{\mathrm{d}t}\xi_{\mathrm{e}} = -\frac{1}{\tau_{\mathrm{B}}}\left(1 - \frac{h^{\|}}{\xi_{\mathrm{e}}}\right)\frac{L(\xi_{\mathrm{e}})}{L'(\xi_{\mathrm{e}})} - \frac{1}{\tau_{\mathrm{N}}}\frac{\xi_{\mathrm{e}}\sinh(\nu)L(\nu)}{\sinh(\xi_{\mathrm{e}})L'(\xi_{\mathrm{e}})\nu^2}\nu^{\|}, \tag{11}$$

where $h^{\|} = \mathbf{h}\cdot\mathbf{n}$ and $\nu^{\|} = \boldsymbol{\nu}\cdot\mathbf{n} = \xi_{\mathrm{e}} - h^{\|}$. Inserting Eq. (11) back into (9), we find

$$\frac{\mathrm{d}}{\mathrm{d}t}\mathbf{n} = \frac{1}{\tau_{\mathrm{B}}}\frac{\xi_{\mathrm{e}} - L(\xi_{\mathrm{e}})}{2\xi_{\mathrm{e}}L(\xi_{\mathrm{e}})}\mathbf{h}^{\perp} - \frac{1}{\tau_{\mathrm{N}}}\frac{\xi_{\mathrm{e}}\sinh(\nu)L(\nu)}{\sinh(\xi_{\mathrm{e}})L(\xi_{\mathrm{e}})\nu^2}\boldsymbol{\nu}^{\perp}, \tag{12}$$

where the components perpendicular to $\mathbf{n}$ are defined by $\mathbf{h}^{\perp} = \mathbf{h} - h^{\|}\mathbf{n}$, $\boldsymbol{\nu}^{\perp} = \boldsymbol{\nu} - \nu^{\|}\mathbf{n}$. Therefore, $\mathrm{d}\mathbf{n}^2/\mathrm{d}t = \mathbf{n}\cdot\mathrm{d}\mathbf{n}/\mathrm{d}t = 0$ and the time evolution (12) ensures that $\mathbf{n}$ remains a unit vector. Equations (11) and (12) represent coupled but closed ordinary differential equations that allow us to determine the effective field $\boldsymbol{\xi}_{\mathrm{e}}(t) = \xi_{\mathrm{e}}(t)\mathbf{n}(t)$ which in turn determines the time-dependent magnetization $\mathbf{m}(t) = L(\xi_{\mathrm{e}}(t))\mathbf{n}(t)$.

To derive more explicit expressions for the late stage characteristic relaxation times, we assume $\mathbf{h}_0 = h_0\hat{\mathbf{h}}$ to

be constant and linearize equations (11) and (12) in the deviation $\boldsymbol{\nu}$ to arrive at $\frac{\mathrm{d}}{\mathrm{d}t}\mathbf{m} = -[S_1 - L(h_0)]\hat{\mathbf{h}}/\tau^{\|} - \mathbf{m}^{\perp}/\tau^{\perp}$ with

$$\frac{1}{\tau^{\|}} = \frac{L(h_0)}{\tau_{\mathrm{B}} h_0 L'(h_0)} + \frac{h_0}{3\tau_{\mathrm{N}} \sinh(h_0) L'(h_0)}, \qquad (13)$$

$$\frac{1}{\tau^{\perp}} = \frac{h_0 - L(h_0)}{2\tau_{\mathrm{B}} L(h_0)} + \frac{h_0^2}{3\tau_{\mathrm{N}} \sinh(h_0) L(h_0)}. \qquad (14)$$

These expressions agree with the ones derived in [77] via perturbation theory. The relaxation times (13) and (14) replace expression (6) for the effective relaxation time in the presence of a constant bias field of strength h_0. For vanishing fields $h_0 \to 0$, Eqs. (13), (14) reduce to Eq. (6). In the rigid-dipole approximation, $\tau_{\mathrm{N}} \to \infty$, the classical result obtained in Ref. [95] is recovered from Eqs. (13), (14). In the opposite limit of frozen dipoles, $\tau_{\mathrm{B}} \to \infty$, the EFA (8) breaks down due to insufficient sampling of orientations and we need to resort to other methods of solution. In Ref. [77], a different ansatz for the pdf was used to derive Brown's result for the effective parallel Néel relaxation time for frozen MNPs from Eq. (7) for large magnetic anisotropy barriers. Since the magnetic anisotropy barrier is included in this model only implicitly via the bare Néel relaxation time τ_{N}, corrections to the asymptotic value for large anisotropies are not captured for any orientation of the field relative to the frozen easy axis [103]. Thus, the DJ model should mainly be used for mobile MNPs.

When a weak oscillatory field $\mathbf{h}_1 = h_1(t)\hat{\mathbf{h}}_1$ with $h_1(t) = h_1 e^{i\omega t}$ is applied in addition to the static field $\mathbf{h}_0$, the complex AC susceptibility becomes anisotropic. Repeating the above calculations with h_0 replaced by $h = h_0 + h_1(t)$ and linearizing in h_1, we obtain explicit expressions for the susceptibilities parallel and perpendicular to the static field direction $\hat{\mathbf{h}}$,

$$\chi_{\|}^* = 3\chi_{\mathrm{L}} L'(h_0) \frac{1 - i\omega\tau^{\|}}{1 + (\omega\tau^{\|})^2}, \qquad (15)$$

$$\chi_{\perp}^* = 3\chi_{\mathrm{L}} \frac{L(h_0)}{h_0} \frac{1 - i\omega\tau^{\perp}}{1 + (\omega\tau^{\perp})^2}, \qquad (16)$$

where χ_{L} denotes the Langevin susceptibility. The susceptibilities (15) and (16) are of the Debye form with field–dependent prefactors. We note that the Debye form is not a consequence of using EFA but results from the linearization about the steady state. In the zero–field and zero–frequency limit, $\chi_{\|}^*$ and $\chi_{\perp}^*$ both become equal to χ_{L}.

B. Expansion in Legendre polynomials

Since the Legendre polynomials $P_n(x)$ form a complete basis for functions on the interval $[-1, 1]$, we can use the following ansatz for the time–dependent pdf [100],

$$f(\mathbf{u}; t) = f_0 + \sum_{n=1}^{\infty} c_n(t) P_n(\mathbf{u} \cdot \hat{\mathbf{h}}), \qquad (17)$$

with $f_0 = 1/(4\pi)$ the isotropic distribution on the unit sphere. The ansatz (17) satisfies the normalization condition $\int f(\mathbf{u}; t)\mathrm{d}\mathbf{u} = 1$ since $\int P_n(\mathbf{u} \cdot \hat{\mathbf{h}})\mathrm{d}\mathbf{u} = 0$ for $n \geq 1$. The expansion coefficients $c_n(t)$ are related to the time–dependent orientational order parameters $S_n(t) = \int P_n(\mathbf{u}\cdot\hat{\mathbf{h}})f(\mathbf{u}; t)\mathrm{d}\mathbf{u}$ introduced above by $S_n(t) = 4\pi c_n(t)/(2n+1)$. We note that the ansatz (17) restricts the pdf to the uniaxial form $f(\mathbf{u}; t) = f(\mathbf{u} \cdot \hat{\mathbf{h}}; t)$, therefore eliminating any dependence on the azimuthal angle. Thus, the ansatz (17) allows us to study only longitudinal dynamics parallel to the field direction.

Inserting the ansatz (17) into the kinetic equation (1) and using the orthogonality relation of Legendre polynomials,

$$\int_{-1}^{1} P_k(x)P_n(x)\mathrm{d}x = \frac{2}{2k+1}\delta_{kn}, \qquad (18)$$

we can express the partial differential equation (1) for the probability density $f(\mathbf{u}; t)$ as an infinite set of coupled ordinary equations for the coefficients $c_n(t)$ as

$$\frac{\mathrm{d}}{\mathrm{d}t}c_n = -\sum_{k=1}^{\infty} A_{nk}c_k + b_n, \qquad (19)$$

where the elements of the matrix $\mathbf{A} = \mathbf{A}_{\mathrm{B}} + \mathbf{A}_{\mathrm{N}}$ are defined by

$$A_{\mathrm{B},nk}(h) = -\int P_n(\mathbf{u} \cdot \hat{\mathbf{h}})\mathrm{L}_{\mathrm{B}}(\mathbf{h})P_k(\mathbf{u} \cdot \hat{\mathbf{h}})\,\mathrm{d}\mathbf{u}, \qquad (20)$$

$$A_{\mathrm{N},nk}(h) = -\int P_n(\mathbf{u} \cdot \hat{\mathbf{h}})\mathrm{L}_{\mathrm{N}}(\mathbf{h})P_k(\mathbf{u} \cdot \hat{\mathbf{h}})\,\mathrm{d}\mathbf{u}. \qquad (21)$$

Since the coefficient c_0 is constant due to the normalization condition, we have separated this contribution into the vector $\mathbf{b} = \mathbf{b}_{\mathrm{B}} + \mathbf{b}_{\mathrm{N}}$ with components

$$b_{\mathrm{B},n}(h) = \int P_n(\mathbf{u} \cdot \hat{\mathbf{h}})\mathrm{L}_{\mathrm{B}}(\mathbf{h})f_0\,\mathrm{d}\mathbf{u} \qquad (22)$$

$$b_{\mathrm{N},n}(h) = \int P_n(\mathbf{u} \cdot \hat{\mathbf{h}})\mathrm{L}_{\mathrm{N}}(\mathbf{h})f_0\,\mathrm{d}\mathbf{u}. \qquad (23)$$

Since details of the derivation of the matrix $\mathbf{A}_{\mathrm{B}}$ can be found e.g. in Refs. [79, 98], we here only give the result,

$$\tau_{\mathrm{B}} A_{\mathrm{B},nk}(h) = n(n+1)\delta_{nk}$$
$$+ \frac{h}{2}\left[\frac{k(k-1)}{2k+1}\delta_{n,k-1} - \frac{(k+1)(k+2)}{2k+1}\delta_{n,k+1}\right] \qquad (24)$$

$$\tau_{\mathrm{B}} b_{\mathrm{B},n}(h) = \frac{h}{3}\delta_{n,1}. \qquad (25)$$

To calculate the matrix elements of $\mathbf{A}_{\mathrm{N}}$ from Eq. (21), we first note that

$$A_{\mathrm{N},nk}(h) = \begin{cases} \frac{(-1)^{k+1}}{\tau_{\mathrm{N}}}E_{nk}(h) & ;\ n \text{ odd} \\ 0 & ;\ n \text{ even} \end{cases} \qquad (26)$$

$$b_{\mathrm{N},n} = \frac{1 - (-1)^n}{4\tau_{\mathrm{N}}}e_n(h), \qquad (27)$$

‌‍‌‌‍‍‍‌‍‌‌‍‍󠀠

where we defined the auxiliary symmetric matrix $\mathbf{E}$ and vector $\mathbf{e}$ as

$$E_{nk}(h) \equiv \int_{-1}^{1} e^{hx} P_n(x) P_k(x) \mathrm{d}x \qquad (28)$$

$$e_n(h) = \int_{-1}^{1} e^{hx} P_n(x) \mathrm{d}x. \qquad (29)$$

For the special case $h = 0$, i.e. no external magnetic field, the Legendre polynomials are eigenfunctions of $\mathsf{L_B}(0) + \mathsf{L_N}(0)$, resulting in a diagonal matrix $\mathbf{A}$. For this special case, the solution can therefore be written as

$$f(\mathbf{u};t) = f_0 + \sum_{n=1}^{\infty} c_n(0) e^{-\lambda_n^0 t} P_n(\mathbf{u} \cdot \hat{\mathbf{h}}), \quad (h = 0) \quad (30)$$

with the zero–field relaxation rates

$$\lambda_n^0 = \begin{cases} \frac{n(n+1)}{2\tau_\mathrm{B}} + \frac{1}{\tau_\mathrm{N}}; & n \text{ odd} \\ \frac{n(n+1)}{2\tau_\mathrm{B}} & n \text{ even.} \end{cases} \qquad (31)$$

We now turn to the general case $h \neq 0$. In this case, the matrix $\mathbf{A}_\mathrm{B}$ is tri–diagonal and linear in h, whereas all entries in odd rows of the matrix $\mathbf{A}_\mathrm{N}$ are non–zero and highly nonlinear in h. While such infinite couplings are in principle problematic for calculations, in practice their magnitude decays rather quickly if h is not too large, allowing us to truncate the infinite system (19).

To evaluate $\mathbf{A}_\mathrm{N}$ and $\mathbf{b}_\mathrm{N}$, the integrals in Eqs. (28) and (29) can be performed numerically for given h. However, doing so for time–dependent fields $h(t)$ becomes computationally expensive for large orders n and k. More efficient expressions for calculating these quantities are provided in A.

IV. RESULTS

We seek solutions to the linear system of equations (19) with time–dependent magnetic fields. In particular, we consider step–changes in the field strength as well as oscillating fields of the form $\mathbf{h}(t) = h(t)\hat{\mathbf{h}}$ with time–dependent amplitude

$$h(t) = h_0 + h_1 \sin(\omega t), \qquad (32)$$

i.e. a superposition of a static field of strength h_0 and an oscillating field with amplitude h_1 and angular frequency ω. Having specified the magnetic field $\mathbf{h}(t)$, Eq. (19) represents an infinite system of coupled linear ODEs with time–dependent coefficients. To solve these equations in practice, we need to truncate this infinite system at some finite order $n_{\max}$. By choosing the value of $n_{\max}$ large enough, the truncation error can be made smaller than a given tolerance. We found that choosing $n_{\max} = 11$ for $h \leq 2$ and $n_{\max} = 15$ for $2 < h \leq 5$ gives very accurate results that are practically indistinguishable from those obtained for larger $n_{\max}$.

A. Spectrum of relaxation times

Diagonalizing the matrix $\mathbf{A}$ in Eq. (19), we find the spectrum of eigenvalues $\{\lambda_1, \lambda_2, \dots\}$, which are the inverses of the corresponding relaxation times. We order the eigenvalues such that $\lambda_1 < \lambda_2 < \dots$, i.e., that the smallest eigenvalue λ_1 corresponds to the longest relaxation time.

We compare the lowest eigenvalue with the late–stage relaxation time within EFA obtained in Sec. III A. From Fig. 1 we find that Eq. (13) provides a good description of λ_1 for weak up to moderate fields, but overpredicts the rates at high field strengths. In other words, EFA underestimates the relaxation times for strong fields. Note that for $q = 0.01$, the prediction from Eq. (13) is indistinguishable on this plot from the rigid dipole approximation where $1/\tau_\mathrm{N} \to 0$.
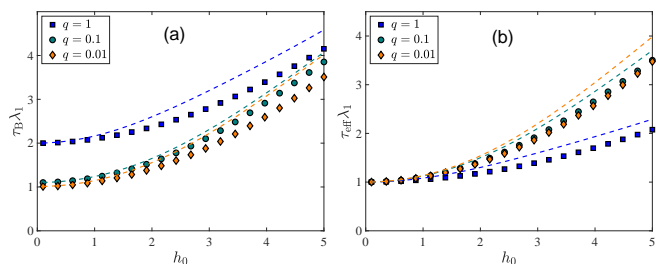

FIG. 1. Lowest eigenvalue λ_1 of the matrix $\mathbf{A}$ in Eq. (19) as a function of the strength of the static field h_0 for different values of q indicated in the legend. In panels (a) and (b), the eigenvalues are normalized with τ_B and τ_eff, respectively. Dashed lines show the EFA result (13).

For the special case of time–independent fields, $\mathbf{h}(t) = \mathbf{h}$, and isotropic initial conditions, $c_k(0) = 0$ for $k \geq 1$, we can use our knowledge of the eigenvalues λ_n to write the analytical solution to Eq. (19) as

$$c_n(t) = \sum_{k=1}^{n_{\max}} w_{nk}(1 - e^{-\lambda_k t}), \qquad (33)$$

where we truncated the infinite sum at $n_{\max}$. The weights w_{nk} appearing in (33) are given by Eq (4.56) in [84],

$$w_{nk} = \sum_{i=1}^{n_{\max}} V_{nk}^{-1} \frac{1}{\lambda_k} V_{ki} b_i, \qquad (34)$$

where the matrix $\mathbf{V}^{-1}$ contains the eigenvectors of $\mathbf{A}$ in its columns.

We are particularly interested in the reduced magnetization (2) with the component parallel to the magnetic field, $S_1(t) = (4\pi/3)c_1(t)$. In Fig. 2 we show the sorted inverse eigenvalues $1/\lambda_k$ together with their weights w_{1k} contributing to the magnetization relaxation, which we calculate from Eq. (34) for different values of h and q. We note that there is no pronounced gap in the spectrum. The second lowest eigenvalue λ_2 is within a factor

5

of two of the lowest eigenvalue λ_1, and similarly for the higher eigenvalues. Also shown in Fig. 2 are the absolute values of the weights w_{1k} defined in (34). We observe that $|w_{1k}|$ increases with h for small k (note the different scales in the different panels in Fig. 2). We note that the absence of a gap in the spectrum is potentially a threat for the validity of closure approximations in terms of the magnetization only, such as EFA. The need for extended closure approximations in the case of magnetically weak MNPs has been discussed in Ref. [77]. However, for the present conditions, the weights are generally found to decrease very fast with increasing k. For weak field strengths, almost all the weight is accumulated at the slowest mode, $k = 1$, implying a near single-exponential magnetization relaxation. For increasing field strengths, the weights for the modes $k = 2$ and $k = 3$ are increasing, implying stronger deviations from single-exponential relaxation. Therefore, we expect the EFA result (13) to be less reliable in this regime, consistent with our observations from Fig. 1.

It is interesting to observe that the ratio $q = \tau_B/\tau_N$ has very little influence on the weights for weak fields $h \lesssim 1$. For stronger field strengths, however, increasing q reduces the weights for the lowest modes and increases the weight of higher order modes, leading to even stronger deviations from single–exponential behavior.
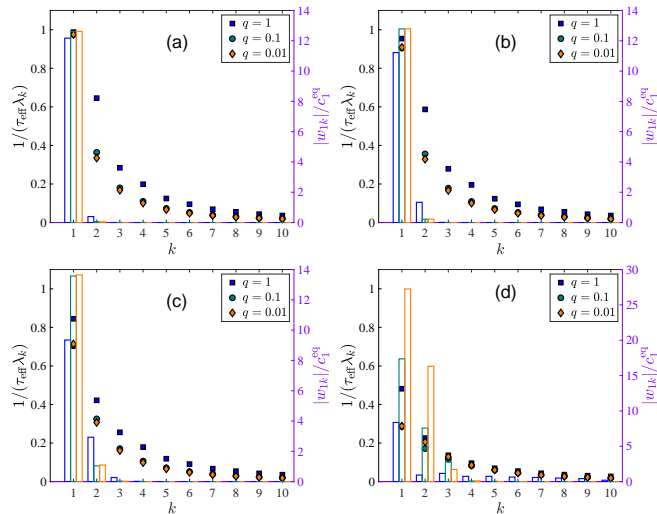

FIG. 2. Symbols show the inverse eigenvalues $1/(\tau_{\text{eff}}\lambda_k)$ of the matrix $\mathbf{A}$ in Eq. (19) normalized with the effective relaxation time τ_{eff}, whereas bars indicate the absolute value of their corresponding weights w_{1k}, Eq. (34). Blue, green, and orange symbols and bars represent results for $q = 1, 0.1$, and 0.01, respectively. In panels (a), (b), (c), (d), the static field h_0 was chosen as $h_0 = 0.5, 1, 2$ and 5, respectively.

B. Transient dynamics following step–change in field strength

In this section, we consider step–changes of the applied magnetic field. Figures 3(a),(b) show the transient dynamics of the orientational order parameters $S_{1,2}(t)$ from an initial isotropic state, $S_k(0) = 0$, $k = 1, 2, \ldots$, after a constant field of strength h has been switched on with $h = 1$ and $h = 5$, respectively. The exact solutions (33) are compared to ensemble averages of stochastic simulations of the DJ model (1). The corresponding algorithm for the stochastic simulations is given in Appendix C. The usual slow convergence of stochastic simulations with ensemble size is seen. For small fields ($h = 0.5$), convergence is found to be rather poor due to pronounced fluctuations. For stronger fields, the signal–to–noise ratio is much more favourable for stochastic simulations. In a sense, stochastic simulations can be considered complementary, since the Legendre expansion is an expansion around the isotropic state and is therefore very efficient for weak fields where stochastic simulations are notoriously noisy. For strong magnetic fields, however, many terms are required in the expansion (17) to represent strongly peaked pdfs. Therefore, the Legendre expansion becomes less efficient for very strong fields where stochastic simulations become more favourable.
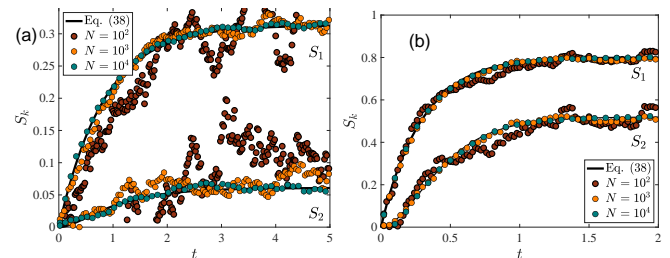

FIG. 3. The orientational order parameters S_1, S_2 as a function of time t after a constant field $h = 1$ (a) and $h = 5$ (b) has been switched on. Isotropic initial conditions have been chosen. The ratio of relaxation times has been chosen as $q = 0.1$. Solid line shows the exact solution (33), while symbols are obtained from stochastic simulations with different ensemble sizes indicated in the legend.

C. Field-dependent AC susceptibility

Consider now longitudinal time–dependent fields $\mathbf{h}(t) = h(t)\hat{\mathbf{h}}$ of the form (32), which for convenience we write as $h(t) = h_0 + h_1 e^{i\omega t}$, where a time-independent bias field h_0 is superimposed to an oscillating field with angular frequncy ω and small amplitude $h_1 \ll 1$. After initial transient dynamics, the expansion coefficients c_k in Eq. (17) are of the form $c_k(t) = c_k^{\text{eq}} + \delta c_k^*(\omega)e^{i\omega t}$ where $c_k^{\text{eq}} = (2k + 1)L_k(h_0)/(4\pi)$, with $L_k(x)$ defined in Eq. (10). The time–dependent deviations from their station-

ary value, $\delta c_k^*(\omega)$, are proportional to h_1 and therefore small.

We rewrite the system of time evolution equations (19) in the compact form $\dot{\mathbf{c}} = -\mathbf{A}(h) \cdot \mathbf{c} + \mathbf{b}(h)$ where we explicitly denote the dependence of $\mathbf{A}$ and $\mathbf{b}$ on the field h. For $h = h_0$, i.e. $h_1 = 0$, we recover the result for c_k^{eq} given above. To first order in h_1, we find that the amplitudes δc_k^* can be calculated as

$$\delta \mathbf{c}^*(\omega) = \frac{h_1}{h_0}[\mathbf{A}(h_0) + i\omega\mathbf{I}]^{-1} \cdot (\mathbf{A}(0) \cdot \mathbf{c}^{\mathrm{eq}} - \mathbf{b}(0)), \quad (35)$$

with $\mathbf{I}$ the identity matrix. Equation (35) agrees with Eq. (4.47) of Ref. [84] for the corresponding solution of the egg model.

We are interested in the induced magnetization $\mathbf{M}_1 = \chi_\parallel^* \mathbf{H}_1$ due to the oscillating field with $\mathbf{M}_1 = M_{\mathrm{sat}}(4\pi/3)\delta c_1^* \hat{\mathbf{h}}$, where $M_{\mathrm{sat}} = n\mu$ denotes the saturation magnetization and $\mathbf{H}_1 = H_1\hat{\mathbf{h}}$ with $h_1 = \mu_0\mu H_1/k_{\mathrm{B}}T$. Therefore, the complex AC susceptibility is given by

$$\chi_\parallel^*(\omega) = 4\pi\chi_{\mathrm{L}}\frac{\delta c_1^*(\omega)}{h_1}, \quad (36)$$

where, as above, $\chi_{\mathrm{L}} = n\mu_0\mu^2/(3k_{\mathrm{B}}T)$ denotes the Langevin susceptibility.

To calculate the susceptibility $\chi_\parallel^*$ we therefore need to obtain $\delta c_1^*(\omega)$ from Eq. (35). Rather than inverting the matrix $\mathbf{A}(h_0) + i\omega\mathbf{I}$ for every frequency ω, we use the diagonalization $\mathbf{A}(h_0) = \mathbf{V}^{-1}\mathbf{\Lambda}\mathbf{V}$, where $\mathbf{\Lambda} = \mathrm{diag}(\lambda_1, \lambda_2, \ldots)$. Thanks to the diagonalization, we can represent the inverse as $[\mathbf{A}(h_0) + i\omega\mathbf{I}]^{-1} = \mathbf{V}^{-1}(\mathbf{\Lambda} + i\omega\mathbf{I})^{-1}\mathbf{V}$ which allows us to conveniently separate real and imaginary part for any ω,

$$(\mathbf{\Lambda} + i\omega\mathbf{I})^{-1} = \mathrm{diag}\left(\frac{\lambda_1 - i\omega}{\lambda_1^2 + \omega^2}, \frac{\lambda_2 - i\omega}{\lambda_2^2 + \omega^2}, \ldots\right). \quad (37)$$

Results for the real and imaginary part of the AC susceptibility obtained from Eq. (36) with the help of Eqs. (35) and (37) are shown in Fig. 4. For weak fields $h \leq 1$, we find that the EFA result (15) provides a rather accurate prediction of the exact results. Furthermore, we observe that the influence of the parameter q can be absorbed mostly by scaling the frequency with the effective relaxation time $\tau_{\mathrm{eff}} = \tau_{\mathrm{B}}/(1 + q)$, defined in Eq. (6). For stronger fields, $h > 1$, the situation is different, with the peak position of $\chi_\parallel''$ moving to higher frequencies more strongly the smaller q. For these stronger fields, the EFA prediction becomes less accurate the larger q. The analogous conclusions have been drawn when discussing the lowest eigenvalues in Fig. 1.

D. Field–dependent response to oscillating magnetic fields

In this section, we apply oscillating magnetic fields of the form $h(t) = h_1 \sin(\omega t)$ with amplitude h_1 and frequency ω. Compared to Sec. IV C, no static bias field
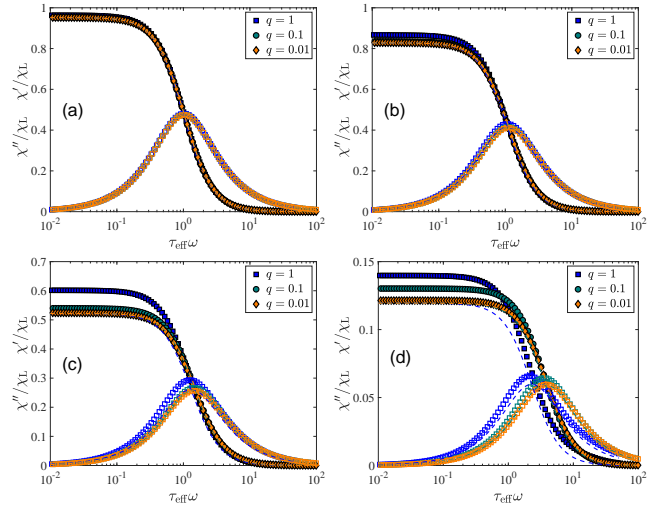

FIG. 4. Real (χ') and complex (χ'') part of the longitudinal dynamic susceptibility $\chi_\parallel^*$ normalized with the Langevin susceptibility χ_{L} are shown as a function of reduced frequency $\tau_{\mathrm{eff}}\omega$. Panels (a), (b), (c), (d) correspond to static fields with strengths $h_0 = 0.5, 1, 2$, and 5, respectively. Dashed lines show the corresponding EFA predictions (15).

is applied here, $h_0 = 0$, and the amplitude h_1 is not restricted to be small. Thus, the response is no longer determined by the dynamic susceptibility χ^* alone.

We solve Eqs. (19) subject to such oscillating magnetic fields for different amplitudes h_1 and frequencies ω. Figure 5 shows the resulting hysteresis curves of the magnetization component parallel to the field direction $S_1(t)$ versus $h(t)$. After a relatively short initial transient, we observe the well–known ellipsoidal shape of the hysteresis curve for weak fields (see Fig. 5(a)). For strong fields, characteristic deviations from the ellipsoidal shape are clearly visible in Fig. 5(b). Note that the shape of the hysteresis curve is also sensitive to the ratio q of relaxation times.
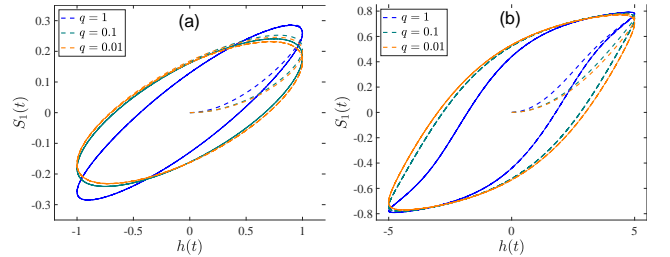

FIG. 5. Hysteresis curves for oscillating magnetic field (32) with $h_0 = 0$, $\tau_{\mathrm{B}}\omega = 1$. The amplitude is chosen as $h_1 = 1$ and $h_1 = 5$ in panel (a) and (b), respectively. Different values for the ratio q are chosen as indicated in the legend.

Oscillating magnetic fields are used in MFH to induce local heating. To study the energy transfer from the magnetic field to the local environment, we follow Ref. [66]

and consider the volumetric power dissipation over one cycle, P, which is given by the area enclosed by the hysteresis curve, $P = \frac{\omega}{2\pi}\mu_0 \oint H \mathrm{d}M$. With $M = M_{\mathrm{sat}}S_1$, where M_{sat} is the saturation magnetization, P can be expressed as

$$P = nk_{\mathrm{B}}T\frac{\omega}{2\pi}\oint h\mathrm{d}S_1. \tag{38}$$

In the linear response regime, i.e. for small enough h_1, the volumetric power dissipation (38) can be calculated as

$$P_{\mathrm{linear}} = \tfrac{1}{6}nk_{\mathrm{B}}T\omega h_1^2\chi_0''(\omega)/\chi_{\mathrm{L}}, \tag{39}$$

where $\chi_0''(\omega)$ denotes the zero-field AC susceptibility. In the absence of a magnetic field, the EFA results (15), (16) reduce to a Debye susceptibility centered at the effective relaxation time τ_{eff} [85],

$$\chi_0''(\omega) = \chi_{\mathrm{L}}\frac{\omega\tau_{\mathrm{eff}}}{1 + (\omega\tau_{\mathrm{eff}})^2}. \tag{40}$$

We note that Eqs. (39) with (40) are routinely used to estimate MFH efficiency, but are valid only for small oscillation amplitudes and non–interacting MNPs [64].

Here, we consider non–interacting MNPs but study a range of amplitudes of the oscillating magnetic field. From the solution to Eq. (19) for $h(t)$, we numerically perform the integral in Eq. (38) over one cycle. To eliminate possible transient effects, we discard the first four cycles. For different frequencies ω, the power absorbed over one cycle P is shown in Fig. 6 as function of the field amplitude h_1. Irrespective of the chosen values for the frequency ω and the ratio q, we find that P increases monotonically with h_1. For high frequencies ($\omega\tau_{\mathrm{B}} = 5$), we find that the linear response result (39) provides rather accurate predictions even for amplitudes up to $h_1 \lesssim 5$. For lower frequencies, however, Eq. (39) is restricted to $h_1 \lesssim 1$ and significantly overpredicts P for larger oscillation amplitudes. It is interesting to note that increasing q decreases $\tau_{\mathrm{eff}}P$ for $\omega\tau_{\mathrm{B}} = 1$, whereas there is a non-monotonic dependence for $\omega\tau_{\mathrm{B}} = 5$.

While a quadratic increase of the power dissipation P with amplitude h_1 is manifest in the linear response regime (39), power-law fits $P \sim h_1^x$ with exponents x larger than two have been reported for some samples in experiments [104]. Figure 7 shows the same data as Fig. 6 but on a double-logarithmic scale. Our results show that non–linearities in the magnetization dynamics typically lead to a decrease of the effective exponent and can not be used to explain values of exponents x significantly larger than two.

E. Tracer response

In this section, we consider general magnetic fields of the form (32) where a bias field h_0 is present in addition to a high–frequency oscillation $h_1\sin(\omega t)$. Different from
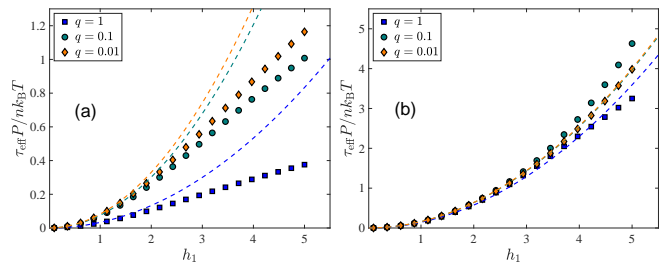

FIG. 6. The dimensionless volumetric power dissipation $P\tau_{\mathrm{eff}}/(nk_{\mathrm{B}}T)$ over one cycle as a function of the amplitude h_1 of the oscillating field. Panels (a) and (b) show the results for frequencies $\omega\tau_{\mathrm{B}} = 1$ and $\omega\tau_{\mathrm{B}} = 5$, respectively. Dashed lines show the linear response result (39).
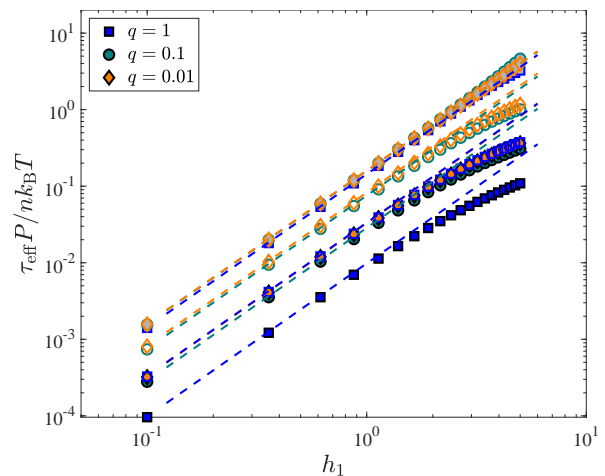

FIG. 7. Data of Fig. 6 are shown on a log-log scale. From bottom to top, the frequency is increasing as $\omega\tau_{\mathrm{B}} = 0.5, 1, 5$.

the situation considered in Sec. IV C, here the amplitude h_1 is not necessarily small.

In MPI, MNPs are detected via their time–dependent magnetization which induces a characteristic signal in pick–up coils. To measure MPI performance of MNP samples, Garraud et al [105] introduced a tracer response quantity defined by the ratio of the time derivative of the induced magnetization over the time derivative of the applied field. Here, we use a dimensionless form of the tracer response,

$$\Upsilon = \frac{\dot{S}_1(t)}{\dot{h}(t)}, \tag{41}$$

which is similar to the quantity studied in [69]. By definition, the tracer response (41) is time–dependent. With an eye on MPI applications, we are particularly interested in relatively high frequencies ω. We therefore consider the time–averaged tracer response $\bar{\Upsilon}$ over one cycle.

In the linear response regime

$$\bar{\Upsilon}_{\text{linear}} = \frac{\chi'_{\parallel}}{3\chi_{\text{L}}} = \frac{L'(h_0)}{1 + (\omega\tau^{\parallel})^2}, \qquad (42)$$

where we used the EFA result (15) in the last equation. Strictly speaking, since the time integral over the additional term proportional to $\chi''_{\parallel}\tan(\omega t)$ appearing in Υ in the linear response regime is ill–behaved, we interpret $\bar{\Upsilon}$ to denote the Cauchy principal value to arrive at (42). Note that the result (42) holds for any strength h_0 of the bias field as long as the amplitudes h_1 of the high–frequency oscillating field are small enough. While the static limit ($\omega = 0$) of (42) was derived in [105], our result includes the full frequency dependence. Note that $\tau^{\parallel} = \tau^{\parallel}(h_0)$ given by Eq. (13) also depends on the strength of the static bias field h_0.

To avoid numerical issues with the tracer response (41) for times t where $\dot{h} = 0$, we use a cubic spline interpolation of the solution to (19) to accurately calculate the time–average of (41) over one cycle. A finite–difference approximation was used to determine $\dot{S}_1$ from the numerical solution $S_1(t)$. As above, we discard the first four cycles to eliminate possible initial transient effects.

Figure 8 shows the time–averaged tracer response $\bar{\Upsilon}$ as a function of the bias field h_0 and the amplitude h_1 of the oscillating field. The linear response result (42) is found to be remarkable accurate for small q where $\bar{\Upsilon}$ is rather insensitive to $h_1 \lesssim 5$ in this regime (see Fig. 8(b)). For large q, however, the linear response result is restricted to $h_1 < 1$, in agreement with our findings in Sec. IV D. In addition, we find from Fig. 8(a) that the dependence on the static field h_0 is well captured by Eq. (42) for small q, but marked differences are seen for $q = 1$.
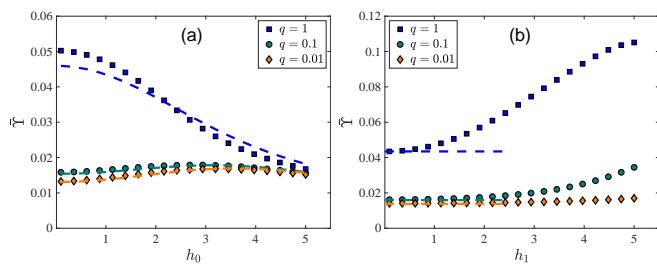

FIG. 8. (a) Dimensionless tracer response (41) averaged over one cycle versus the magnitude h_0 of a static bias field which was applied in addition to an oscillating field with amplitude $h_1 = 1$ and frequency $\omega\tau_{\text{eff}} = 5$. (b) Same quantity but shown versus the amplitude h_1 of the oscillating field for a fixed value of the constant bias field $h_0 = 1$. The frequency was again chosen as $\omega\tau_{\text{eff}} = 5$. Dashed lines show the linear response result (42).

V. DISCUSSION

In this study, we have employed the DJ model [85] to explore the nonequilibrium response of MNPs to time–varying magnetic fields beyond the linear regime over a broad range of parameter values. Extending previous works, we study different ratios of the basic Brownian and Néel relaxation times and their influence on the magnetization dynamics for different field strengths and frequencies. We establish quasi–exact solutions to the longitudinal dynamics of the model in terms of an expansion in Legendre polynomials. We also derive approximate analytical results from dynamical mean-field theory. The widely used EFA is found to provide accurate predictions when Brownian relaxations dominate, but becomes less reliable the stronger the Néel contribution.

It is important to point out that treating the combined effect of Brownian and Néel processes as a single–exponential relaxation with effective relaxation time τ_{eff} given in Eq. (6) is valid only for non–interacting MNPs in the absence of external fields. With increasing strength of an applied magnetic field, deviations from single–exponential behavior become more and more pronounced (see Fig. 2). It is remarkable that the relative weights of the higher–order relaxation modes provide a fingerprint of the underlying mechanism since they depend on the ratio q of the characteristic Brownian to Néel relaxation time.

Within the DJ model, Néel relaxation processes are modelled as independent and thermally activated events following a Poisson statistics. Instead, one could consider the more microscopic egg model [79, 80] where internal relaxation is modelled using the stochastic Landau–Lifshitz–Gilbert equation coupled to Brownian particle rotation. While the DJ model was first proposed phenomenologically [85], it was later shown [77] to provide rather accurate results when compared to the microscopic egg model for large magnetic anisotropies ("magnetically hard" MNPs). We emphasize that this limit corresponds to thermally activated Néel relaxation, as indeed assumed in the DJ model. Note that the egg model is highly inefficient in this regime since the underlying Landau–Lifshitz–Gilbert equation resolves the attempt frequencies on time scales $\tau_0 \sim 10^{-10}$s, which is much smaller than the Néel time scale τ_{N} for magnetization reversals for large anisotropy barriers as well as typical values for τ_{B} [94]. Therefore, the success of the DJ model relies on the time scale separation $\tau_0 \ll \tau_{\text{B}}, \tau_{\text{N}}$, which allows us to neglect processes on fast time scale τ_0 when we are interested in long-time dynamics. For MNPs with small magnetic anisotropies, on the other hand, $\tau_0 \sim \tau_{\text{N}}$, which undermines the assumptions made in the DJ model and one needs to resort to the egg model to resolve these short time scales.

Another deliberate limitation of the present study is the focus on non–interacting MNPs. While a large number of experiments are performed in very dilute conditions, the importance of dipolar interactions for larger

concentrations is well known [56, 106]. Exploring the enlarged parameter space with additional interaction effects via detailed computer simulations is very challenging when Néel and Brownian processes are both kept. Some first steps in this direction have been made recently [86, 88, 94, 107].

VI. CONCLUSIONS

Detailed understanding the field–induced nonequilibrium dynamics of MNPs is crucial for developing and optimizing a variety of technical and biomedical applications. In view of the large parameter space, many researcher resort to highly simplified linear equilibrium models. Here, we show that the more realistic DJ model is able to describe the fully nonequilibrium and non–linear field–induced dynamics resulting from the combined Brownian and Néel relaxation at moderate computational cost. We also provide approximate analytical expressions for effective field–dependent relaxation times, dynamic magnetic susceptibilities, volumetric power dissipation, and tracer response.

The DJ model is restricted to magnetically hard MNPs where Néel relaxation can be treated as rare, thermally activated magnetization reversals. The efficient modelling in this parameter regime also allows us to study concentration and interaction effects via detailed simulations using a straightforward generalization of the DJ model [88, 107]. Furthermore, the DJ model could also be helpful for other applications, e.g. to estimate the local temperature from MNP relaxation by extending the analysis proposed by Perreard *et al* [108] beyond the rigid–dipole approximation.

Appendix A: Calculating the quantities E and e efficiently

Using the well–known recursion formula for Legendre polynomials, $(n + 1)P_{n+1}(x) = (2n + 1)xP_n(x) - nP_{n-1}(x)$, we can derive a recursion formula for the functions $e_n(h)$ defined in Eq. (29),

$$e_{n+1}(h) = e_{n-1}(h) - \frac{2n+1}{h}e_n(h), \qquad (A1)$$

where $e_0(h) = 2\sinh(h)/h$ and $e_1(h) = (2/h^2)[h\cosh(h) - \sinh(h)]$. While formally exact, we found that the recursion relation (A1) becomes numerically unstable for small h at large orders n. Instead, we find the exact expression

$$e_n(h) = \frac{2\sinh(h)I_{n+1/2}(h)}{h\,I_{1/2}(h)} \qquad (A2)$$

in terms of modified Bessel functions to be more stable numerically. For very small $h \ll 1$, $e_n(h)$ vanish smoothly and can be approximated by $e_0(h) = 2 + (1/3)h^2 + \mathcal{O}(h^4)$, $e_1(h) = (2/3)h + \mathcal{O}(h^3)$, $e_2(h) = (2/15)h^2 + \mathcal{O}(h^4)$ and $e_k(h) = \mathcal{O}(h^k)$ can be neglected for $k \geq 3$.

Unfortunately, we could not find a corresponding analytic expression for $E_{nk}(h)$ valid for arbitrary h. Instead, we suggest to use a classical formula for the product of two Legendre polynomials [109],

$$P_n(x)P_k(x) = \sum_{\ell=|n-k|}^{n+k} \begin{pmatrix} \ell & n & k \\ 0 & 0 & 0 \end{pmatrix}^2 (2\ell + 1)P_\ell(x), \quad (A3)$$

with the Wigner $(3j)$ symbol

$$\begin{pmatrix} \ell & n & k \\ 0 & 0 & 0 \end{pmatrix}^2 = \frac{(2s - 2\ell)!(2s - 2n)!(2s - 2k)!}{(2s + 1)!} \left[\frac{s!}{(s - \ell)!(s - n)!(s - k)!} \right]^2, \qquad (A4)$$

where $2s = \ell + k + n$ must be even and ℓ, n, k satisfy the triangle inequality $|a - b| < c < a + b$, otherwise the Wigner $(3j)$ symbol is zero. With the help of (A3), we can write the matrix elements (28) as

$$E_{nk}(h) = \sum_{\ell=|n-k|}^{n+k} \begin{pmatrix} \ell & n & k \\ 0 & 0 & 0 \end{pmatrix}^2 (2\ell + 1)e_\ell(h), \qquad (A5)$$

with $e_\ell(h)$ defined in Eq. (29). Therefore, knowledge of the integrals (29) from Eq. (A2) is sufficient to build all the matrix elements of $\mathbf{A}_N$ via Eqs. (A5) and (26). In Sec. B, we provide the explicit expressions for the first elements of $\mathbf{A}_N$ and $\mathbf{b}_N$.

Appendix B: Analytical expression for some matrix elements

The exact expressions for the first four elements of the vector $\mathbf{b}$ defined in Eqs. (22) and (23) read

$$b_1(h) = \frac{h}{3\tau_B} + \frac{1}{\tau_N h^2}[h\cosh(h) - \sinh(h)]$$

$$b_2(h) = 0$$

$$b_3(h) = \frac{1}{\tau_N h^4}[h(15 + h^2)\cosh(h) - 3(5 + 2h^2)\sinh(h)]$$

$$b_4(h) = 0.$$

The first elements of the matrix $\mathbf{A}_N$ defined in Eq. (21) read explicitly

$$A_{N,11}(h) = \frac{2}{\tau_N h^3}[(2 + h^2)\sinh(h) - 2h\cosh(h)]$$

$$A_{N,12}(h) = -\frac{2}{\tau_N h^4}[h(9 + h^2)\cosh(h) - 2(9 + 4h^2)\sinh(h)]$$

$$A_{N,13}(h) = \frac{2}{\tau_N h^5}\big[(60 + 27h^2 + h^4)\sinh(h)$$
$$- h(60 + 7h^2)\cosh(h)\big]$$

$$A_{N,21}(h) = -A_{N,12}(h)$$

$$A_{N,22}(h) = -\frac{2}{\tau_N h^5}\big[(54 + 24h^2 + h^4)\sinh(h)$$
$$- 6h(9 + h^2)\cosh(h)\big]$$

$$A_{N,23}(h) = \frac{2}{\tau_N h^6}\big[h(450 + 54h^2 + h^4)\cosh(h)$$
$$- 3(150 + 68h^2 + 3h^4)\sinh(h)\big]$$

$$A_{N,31}(h) = A_{N,13}(h)$$

$$A_{N,32}(h) = -A_{N,23}(h)$$

$$A_{N,33}(h) = \frac{2}{\tau_N h^7}\big[(4500 + 2070h^2 + 102h^4 + h^6)\sinh(h)$$
$$- 6h(10 + h^2)(75 + 2h^2)\cosh(h)\big].$$

Appendix C: Stochastic simulations of the diffusion-jump model

We here collect the essential ingredients for the stochastic simulation of the diffusion–jump model (1). More details can be found in Ref. [88] which also covers the interacting many-body generalization of the model.

Using a small time step Δt, we can use operator splitting methods to approximate the solution to Eq. (1) as

$$f(\mathbf{u}; t + \Delta t) \approx (1 + \Delta t\, \mathsf{L}_N)e^{\Delta t\, \mathsf{L}_B} f(\mathbf{u}; t). \quad \text{(C1)}$$

Therefore, in one time step Δt, we first propagate the system according to the Fokker–Planck operator L_B before applying the jump operator L_N. Representing the pdf $f(\mathbf{u}; t)$ by an ensemble of N unit vectors $\{\mathbf{u}_t\}$, we use the well–known equivalence between Fokker-Planck and stochastic differential equations [110] to perform one time step of rotational Brownian Dynamics [97, 110],

$$\mathbf{u}_t \to \mathbf{u}'_t = \frac{\mathbf{u}_t + \Delta\boldsymbol{\Omega}_t \times \mathbf{u}_t}{|\mathbf{u}_t + \Delta\boldsymbol{\Omega}_t \times \mathbf{u}_t|}, \quad \text{(C2)}$$

where the increment in angular velocity is given by $\Delta\boldsymbol{\Omega}_t = \Delta t/(2\tau_B)\mathbf{u}_t \times \mathbf{h}(t) + \Delta\mathbf{W}_t$ with $\Delta\mathbf{W}_t$ increments of a three-dimensional Wiener process with zero mean and variance $1/\tau_B$. In fact, for the results shown here, we use a second order Heun algorithm [110] where Eq. (C2) serves as the predictor step.

To implement the jump process associated with the operator L_N, we define the rate $r_t = e^{-\mathbf{u}'_t \cdot \mathbf{h}(t)}/(2\tau_N)$ and use the characteristic property of Poisson processes that the probability of no event occurring in the time interval $[t, t + \Delta t]$ is given by $e^{-r_t \Delta t}$. Therefore, we reverse the magnetic moment $\mathbf{u}'_t \to -\mathbf{u}'_t$ with probability $1 - e^{-r_t \Delta t}$. Thus, to complete one time step of the stochastic simulation algorithm we set

$$\mathbf{u}_{t+\Delta t} = \begin{cases} \mathbf{u}'_t & \text{for } \zeta < e^{-r_t \Delta t} \\ -\mathbf{u}'_t & \text{for } \zeta \geq e^{-r_t \Delta t} \end{cases} \quad \text{(C3)}$$

where $\zeta \in [0, 1]$ is a uniform random number.

Updating the ensemble of unit vector $\{\mathbf{u}_t\}$ by repeating the steps (C2) and (C3) provides an algorithm for stochastic simulations of the DJ model. This hybrid scheme combines Brownian Dynamics (C2) and kinetic Monte–Carlo–type (C3) schemes. For the simulation results shown above, we use a time step of $\Delta t = 10^{-3}\tau_B$.

[1] S. Odenbach, editor. *Colloidal Magnetic Fluids*, volume 763 of *Lecture Notes in Phys.* Springer, Berlin, 2009. I, II A, II A, V

[2] V. Socoliuc, M. V. Avdeev, V. Kuncser, Rodica Turcu, Etelka Tombácz, and L. Vékás. Ferrofluids and bio-ferrofluids: looking back and stepping forward. *Nanoscale*, 14(13):4786–4886, 2022. I

[3] Vanessa Fernandes Cardoso, António Francesko, Clarisse Ribeiro, Manuel Bañobre-López, Pedro Martins, and Senentxu Lanceros-Mendez. Advances in magnetic nanoparticles for biomedical applications. *Advanced Healthcare Materials*, 7(5):1700845–35, 2017. Publisher: John Wiley & Sons, Ltd.

[4] Q. A. Pankhurst, N. T. K. Thanh, S. K. Jones, and J. Dobson. Progress in applications of magnetic particles in biomedicine. *J. Phys. D: Appl. Phys.*, 42:224001,

2009. I

[5] Angelie Rivera-Rodriguez and Carlos M. Rinaldi-Ramos. Emerging biomedical applications based on the response of magnetic nanoparticles to time-varying magnetic fields. *Annual Review of Chemical and Biomolecular Engineering*, 12(1):163–185, 2021. I

[6] Dietmar Eberbeck, Christian Bergemann, Stefan Hartwig, Uwe Steinhoff, and Lutz Trahms. Binding kinetics of magnetic nanoparticles on latex beads and yeast cells studied by magnetorelaxometry. *Journal Of Magnetism And Magnetic Materials*, 289:435–438, March 2005. I

[7] Frank Wiekhorst, Uwe Steinhoff, Dietmar Eberbeck, and Lutz Trahms. Magnetorelaxometry Assisting Biomedical Applications of Magnetic Nanoparticles. *Pharmaceutical research*, 29(5):1189–1202, 2012. I

[8] David Chang, May Lim, Jeroen A C M Goos, Ruirui Qiao, Yun Yee Ng, Friederike M Mansfeld, and Michael Jackson. Biologically Targeted Magnetic Hyperthermia: Potential and Limitations. *Frontiers in Pharmacology*, 9:831, August 2018. I

[9] Silvio Dutz and Rudolf Hergt. Magnetic particle hyperthermia—a promising tumour therapy? *Nanotechnology*, 25(45):452001, November 2014. I, IV D

[10] Cindi L Dennis and Robert Ivkov. Physics of heat generation using magnetic nanoparticles for hyperthermia. *International Journal of Hyperthermia*, 29(8):715–729, November 2013.

[11] R E Rosensweig. Heating magnetic fluid with alternating magnetic field. *Journal of Magnetism and Magnetic Materials*, 252:370–374, November 2002. I, II B, IV D

[12] Bernhard Gleich and Jürgen Weizenecker. Tomographic imaging using the nonlinear response of magnetic particles. *Nature*, 435(7046):1214–1217, 2005. Publisher: Nature Publishing Group. I

[13] Zhi Wei Tay, Shehaab Savliwala, Daniel W. Hensley, K.L. Barry Fung, Caylin Colson, Benjamin D. Fellows, Xinyi Zhou, Quincy Huynh, Yao Lu, Bo Zheng, Prashant Chandrasekharan, Sindia M. Rivera-Jimenez, Carlos M. Rinaldi-Ramos, and Steven M. Conolly. Superferromagnetic nanoparticles enable order-of-magnitude resolution & sensitivity gain in magnetic particle imaging. *Small Methods*, 5(11):2100796, 2021.

[14] Zhiyuan Zhao and Carlos Rinaldi. Computational predictions of enhanced magnetic particle imaging performance by magnetic nanoparticle chains. *Physics in Medicine & Biology*, 65(18):185013, 2020. IV E

[15] T Knopp, N Gdaniec, and M Möddel. Magnetic particle imaging: from proof of principle to preclinical applications. *Physics in Medicine & Biology*, 62(14):R124–R178, 2017. I

[16] Jörn Borgert, Joachim D Schmidt, Ingo Schmale, Claas Bontus, Bernhard Gleich, Bernd David, Jürgen Weizenecker, Jonas Jockram, Christian Lauruschkat, Oliver Mende, Mathias Heinrich, Aleksi Halkola, Jörn Bergmann, Oliver Woywode, and Jürgen Rahmer. Perspectives on clinical magnetic particle imaging. *Biomedical Engineering / Biomedizinische Technik*, 58(6):551–556, 2013. Publisher: De Gruyter. I

[17] Stanley Harvell-Smith, Le Duc Tung, and Nguyen Thi Kim Thanh. Magnetic particle imaging: tracer development and the biomedical applications of a radiation-free, sensitive, and quantitative imaging modality. *Nanoscale*, 14(10):3658–3697, 2022. I

[18] R Matthew Ferguson, Kevin R Minard, Amit P Khandhar, and Kannan M Krishnan. Optimizing magnetite nanoparticles for mass sensitivity in magnetic particle imaging. *Med. Phys.*, 38(3):1619–1626, March 2011. I

[19] Asahi Tomitaka, Satoshi Ota, Kizuku Nishimoto, Hamed Arami, Yasushi Takemura, and Madhavan Nair. Dynamic magnetic characterization and magnetic particle imaging enhancement of magnetic-gold core–shell nanoparticles. *Nanoscale*, 11(13):6489–6496, 2019. I

[20] Alison E. Deatsch and Benjamin A. Evans. Heating efficiency in magnetic nanoparticle hyperthermia. *Journal of Magnetism and Magnetic Materials*, 354:163–172, 2014. I

[21] Robert J. Deissler, Yong Wu, and Michael A. Martens. Dependence of Brownian and Néel relaxation times on magnetic field strength. *Med. Phys.*, 41(1):012301, 2014. I

[22] Patrick Ilg and Martin Kröger. Longest relaxation time versus maximum loss peak in the field-dependent longitudinal dynamics of suspended magnetic nanoparticles. *Physical Review B*, 106(13):134433, 2022. I, II A, III, III A, III A, III A, IV A, V

[23] Carolyn Shasha and Kannan M. Krishnan. Nonequilibrium dynamics of magnetic nanoparticles with applications in biomedicine. *Advanced Materials*, 33(23):1904131, 2021. I

[24] W T Coffey, P J Cregg, and Yu P Kalmykov. On the theory of Debye and Neel relaxation of single domain ferromagnetic particles. In I Prigogine and S A Rice, editors, *Advances in Chemical Physics*, pages 263–464. John Wiley & Sons, 1993. I, II A, III B, V

[25] M.I. Shliomis and V.I. Stepanov. Theory of the dynamic susceptibility of magnetic fluids. In William Coffey, editor, *Relaxation Phenomena in Condensed Matter*, volume LXXXVII of *Advances in Chemical Physics*, pages 1–30. John Wiley & Sons, 1994. I, II A, V

[26] Henrik Rogge, Marlitt Erbe, Thorsten M Buzug, and Kerstin Lüdtke-Buzug. Simulation of the magnetization dynamics of diluted ferrofluids in medical applications. *Biomedizinische Technik/Biomedical Engineering*, 58(6):1–9, November 2013. I

[27] Daniel B Reeves and John B Weaver. Combined Néel and Brown rotational Langevin dynamics in magnetic particle imaging, sensing, and therapy. *Applied Physics Letters*, 107(22):223106, December 2015. I

[28] I.S. Poperechny. Combined rotational diffusion of a superparamagnetic particle and its magnetic moment: Solution of the kinetic equation. *J Molec Liq*, 299:112109, 2020. I

[29] Martin Kröger and Patrick Ilg. Combined dynamics of magnetization and particle rotation of a suspended superparamagnetic particle in the presence of an orienting field: Semi-analytical and numerical solution. *Math. Models Meth. Appl. Sci.*, 32(7):1–35, 2022. I, IV A, IV C

[30] Patrick Ilg. Diffusion-jump model for the combined Brownian and Néel relaxation dynamics of ferrofluids in the presence of external fields and flow. *Physical Review E*, 100(2):022608, August 2019. I, II A, II A, II B, II B, III, IV D, V

[31] D. V. Berkov, N. L. Gorn, R. Schmitz, and D. Stock. Langevin dynamic simulations of fast remagnetization processes in ferrofluids with internal magnetic degrees of freedom. *J. Phys.: Condens. Matter*, 18:S2595–S2621, 2006. I, II A, II A, V

[32] C. Haase and U. Nowak. Role of dipole-dipole interactions for hyperthermia heating of magnetic nanoparticle ensembles. *Physical Review B*, 85(4):045435, 2012.

[33] P Ilg and M Kröger. Dynamics of interacting magnetic nanoparticles: effective behavior from competition between Brownian and Néel relaxation. *Phys. Chem. Chem. Phys.*, 22:22244–22259, 2020. I, V, VI, C

[34] Fannin, P.C. and S W Charles. The study of a ferrofluid exhibiting both Brownian and Neel relaxation. *Journal of Physics D Applied Physics*, 22(1):187–191, January 1989. II A

[35] J.-O. Andersson, C. Djurberg, T. Jonsson, P. Svedlindh, and P. Nordblad. Monte carlo studies of the dynamics of an interacting monodispersive magnetic-particle system. *Phys. Rev. B*, 56(21):13983–13988, 1997. II A

[36] J Carrey, B Mehdaoui, and M Respaud. Simple models for dynamic hysteresis loop calculations of magnetic single-domain nanoparticles: Application to magnetic hyperthermia optimization. *Journal Of Applied Physics*, 109(8):083921, April 2011.

[37] S Ruta, R Chantrell, and O Hovorka. Unified model of hyperthermia via hysteresis heating in systems of interacting magnetic nanoparticles. *Scientific Reports*, 5:9090–7, March 2015.

[38] Christian Jonasson, Vincent Schaller, Lunjie Zeng, Eva Olsson, Cathrine Frandsen, Alejandra Castro, Lars Nilsson, Lara K Bogart, Paul Southern, Quentin A Pankhurst, M Puerto Morales, and Christer Johansson. Modelling the effect of different core sizes and magnetic interactions inside magnetic nanoparticles on hyperthermia performance. *Journal of Magnetism and Magnetic Materials*, 477:198–202, May 2019. II A

[39] D. V. Berkov, N. L. Gorn, and D. Stock. Combined Langevin dynamics/Monte-Carlo simulations of the non-equilibrium ferrofluid remagnetization. *J. Magn. Magn. Mater.*, 272:E1281–E1283, 2004. II A, V

[40] M. A. Martsenyuk, Yu. L. Raikher, and M. I. Shliomis. On the kinetics of magnetization of suspension of ferromagnetic particles. *Sov. Phys. JETP*, 38(2):413–416, 1974. II B, III A, III A, III A

[41] J. T. Waldron, Yu. P. Kalmykov, and W. T. Coffey. Rotational Brownian motion and dielectric relaxation of polar molecules subjected to constant bias field: Exact solution. *Phys. Rev. E*, 49(5):3976–3989, 1994. II B

[42] P. Ilg, M. Kröger, and S. Hess. Magnetoviscosity and orientational order parameters of dilute ferrofluids. *J. Chem. Phys.*, 116(20):9078–9088, 2002. III A, C

[43] B U Felderhof and R B Jones. Nonlinear response of a dipolar system with rotational diffusion to an oscillating field. *J. Phys.: Condens. Matter*, 15(15):S1363–S1378, 2003. III B

[44] Jorge H. Sánchez and Carlos Rinaldi. Magnetoviscosity of dilute magnetic fluids in oscillating and rotating magnetic fields. *Physics of Fluids*, 22(4):043304, 2010. II B

[45] M. Kröger. Simple models for complex nonequilibrium fluids. *Phys. Rep.*, 390(6):453–551, 2004. III, III B

[46] Yu. L. Raikher and M. I. Shliomis. The effective field method in the orientational kinetics of magnetic fluids. *Adv. Chem. Phys.*, 87:595, 1994. III A

[47] P. Ilg, M. Kröger, S. Hess, and A. Yu. Zubarev. Dynamics of colloidal suspensions of ferromagnetic particles in plane Couette flow: Comparison of approximate solutions with Brownian dynamics simulations. *Phys. Rev.*

[48] W T Coffey, D S F Crothers, J L Dorman, L J Geoghegan, Yu. P. Kalmykov, J T Waldron, and A W Wickstead. Effect of an oblique magnetic field on the superparamagnetic relaxation time. *Phys. Rev. B*, 52(22):15951, 1995. III A

[49] M. Cobianchi, A. Guerrini, M. Avolio, C. Innocenti, M. Corti, P. Arosio, F. Orsini, C. Sangregorio, and A. Lascialfari. Experimental determination of the frequency and field dependence of specific loss power in magnetic fluid hyperthermia. *Journal of Magnetism and Magnetic Materials*, 444:154–160, 2017. IV D

[50] Nicolas Garraud, Rohan Dhavalikar, Mythreyi Unni, Shehaab Savliwala, Carlos Rinaldi, and David P Arnold. Benchtop magnetic particle relaxometer for detection, characterization and analysis of magnetic nanoparticles. *Physics in Medicine & Biology*, 63(17):175016, 2018. IV E, IV E

[51] Maheshika Palihawadana-Arachchige, Humeshkar Nemala, Vaman M Naik, and Ratna Naik. Effect of magnetic dipolar interactions on temperature dependent magnetic hyperthermia in ferrofluids. *Journal Of Applied Physics*, 121(2):023901, January 2017. V

[52] Patrick Ilg and Martin Kröger. Field- and concentration-dependent relaxation of magnetic nanoparticles and optimality conditions for magnetic fluid hyperthermia. *Scientific Reports*, 13:16523, 2023. V, VI

[53] I M Perreard, D B Reeves, X Zhang, E Kuehlert, E R Forauer, and J B Weaver. Temperature of the magnetic nanoparticle microenvironment: estimation from relaxation times. *Phys. Med. Biol.*, 59(5):1109–1119, 2014. Publisher: IOP Publishing. VI

[54] J C Adams. III. On the expression of the product of any two Legendre's coefficients by means of a series of Legendre's coefficients. *Proceedings Of The Royal Society Of London*, 27(185):63–71, 1878. A

[55] H. C. Öttinger. *Stochastic Processes in Polymeric Fluids.* Springer, Berlin, 1996. C, C

[56] S. Odenbach, editor. *Colloidal Magnetic Fluids*, volume 763 of *Lecture Notes in Phys.* Springer, Berlin, 2009. I, II A, II A, V

[57] V. Socoliuc, M. V. Avdeev, V. Kuncser, Rodica Turcu, Etelka Tombácz, and L. Vékás. Ferrofluids and bio-ferrofluids: looking back and stepping forward. *Nanoscale*, 14(13):4786–4886, 2022. I

[58] Vanessa Fernandes Cardoso, António Francesko, Clarisse Ribeiro, Manuel Bañobre-López, Pedro Martins, and Senentxu Lanceros-Mendez. Advances in magnetic nanoparticles for biomedical applications. *Advanced Healthcare Materials*, 7(5):1700845–35, 2017. Publisher: John Wiley & Sons, Ltd.

[59] Q. A. Pankhurst, N. T. K. Thanh, S. K. Jones, and J. Dobson. Progress in applications of magnetic particles in biomedicine. *J. Phys. D: Appl. Phys.*, 42:224001, 2009. I

[60] Angelie Rivera-Rodriguez and Carlos M. Rinaldi-Ramos. Emerging biomedical applications based on the response of magnetic nanoparticles to time-varying magnetic fields. *Annual Review of Chemical and Biomolecular Engineering*, 12(1):163–185, 2021. I

[61] Dietmar Eberbeck, Christian Bergemann, Stefan Hartwig, Uwe Steinhoff, and Lutz Trahms. Binding

kinetics of magnetic nanoparticles on latex beads and yeast cells studied by magnetorelaxometry. *Journal Of Magnetism And Magnetic Materials*, 289:435–438, March 2005. I

[62] Frank Wiekhorst, Uwe Steinhoff, Dietmar Eberbeck, and Lutz Trahms. Magnetorelaxometry Assisting Biomedical Applications of Magnetic Nanoparticles. *Pharmaceutical research*, 29(5):1189–1202, 2012. I

[63] David Chang, May Lim, Jeroen A C M Goos, Ruirui Qiao, Yun Yee Ng, Friederike M Mansfeld, and Michael Jackson. Biologically Targeted Magnetic Hyperthermia: Potential and Limitations. *Frontiers in Pharmacology*, 9:831, August 2018. I

[64] Silvio Dutz and Rudolf Hergt. Magnetic particle hyperthermia—a promising tumour therapy? *Nanotechnology*, 25(45):452001, November 2014. I, IV D

[65] Cindi L Dennis and Robert Ivkov. Physics of heat generation using magnetic nanoparticles for hyperthermia. *International Journal of Hyperthermia*, 29(8):715–729, November 2013.

[66] R E Rosensweig. Heating magnetic fluid with alternating magnetic field. *Journal of Magnetism and Magnetic Materials*, 252:370–374, November 2002. I, II B, IV D

[67] Bernhard Gleich and Jürgen Weizenecker. Tomographic imaging using the nonlinear response of magnetic particles. *Nature*, 435(7046):1214–1217, 2005. Publisher: Nature Publishing Group. I

[68] Zhi Wei Tay, Shehaab Savliwala, Daniel W. Hensley, K.L. Barry Fung, Caylin Colson, Benjamin D. Fellows, Xinyi Zhou, Quincy Huynh, Yao Lu, Bo Zheng, Prashant Chandrasekharan, Sindia M. Rivera-Jimenez, Carlos M. Rinaldi-Ramos, and Steven M. Conolly. Superferromagnetic nanoparticles enable order-of-magnitude resolution & sensitivity gain in magnetic particle imaging. *Small Methods*, 5(11):2100796, 2021.

[69] Zhiyuan Zhao and Carlos Rinaldi. Computational predictions of enhanced magnetic particle imaging performance by magnetic nanoparticle chains. *Physics in Medicine & Biology*, 65(18):185013, 2020. IV E

[70] T Knopp, N Gdaniec, and M Möddel. Magnetic particle imaging: from proof of principle to preclinical applications. *Physics in Medicine & Biology*, 62(14):R124–R178, 2017. I

[71] Jörn Borgert, Joachim D Schmidt, Ingo Schmale, Claas Bontus, Bernhard Gleich, Bernd David, Jürgen Weizenecker, Jonas Jockram, Christian Lauruschkat, Oliver Mende, Mathias Heinrich, Aleksi Halkola, Jörn Bergmann, Oliver Woywode, and Jürgen Rahmer. Perspectives on clinical magnetic particle imaging. *Biomedical Engineering / Biomedizinische Technik*, 58(6):551–556, 2013. Publisher: De Gruyter. I

[72] Stanley Harvell-Smith, Le Duc Tung, and Nguyen Thi Kim Thanh. Magnetic particle imaging: tracer development and the biomedical applications of a radiation-free, sensitive, and quantitative imaging modality. *Nanoscale*, 14(10):3658–3697, 2022. I

[73] R Matthew Ferguson, Kevin R Minard, Amit P Khandhar, and Kannan M Krishnan. Optimizing magnetite nanoparticles for mass sensitivity in magnetic particle imaging. *Med. Phys.*, 38(3):1619–1626, March 2011. I

[74] Asahi Tomitaka, Satoshi Ota, Kizuku Nishimoto, Hamed Arami, Yasushi Takemura, and Madhavan Nair. Dynamic magnetic characterization and magnetic particle imaging enhancement of magnetic-gold core–shell nanoparticles. *Nanoscale*, 11(13):6489–6496, 2019. I

[75] Alison E. Deatsch and Benjamin A. Evans. Heating efficiency in magnetic nanoparticle hyperthermia. *Journal of Magnetism and Magnetic Materials*, 354:163–172, 2014. I

[76] Robert J. Deissler, Yong Wu, and Michael A. Martens. Dependence of Brownian and Néel relaxation times on magnetic field strength. *Med. Phys.*, 41(1):012301, 2014. I

[77] Patrick Ilg and Martin Kröger. Longest relaxation time versus maximum loss peak in the field-dependent longitudinal dynamics of suspended magnetic nanoparticles. *Physical Review B*, 106(13):134433, 2022. I, II A, III, III A, III A, III A, IV A, V

[78] Carolyn Shasha and Kannan M. Krishnan. Nonequilibrium dynamics of magnetic nanoparticles with applications in biomedicine. *Advanced Materials*, 33(23):1904131, 2021. I

[79] W T Coffey, P J Cregg, and Yu P Kalmykov. On the theory of Debye and Neel relaxation of single domain ferromagnetic particles. In I Prigogine and S A Rice, editors, *Advances in Chemical Physics*, pages 263–464. John Wiley & Sons, 1993. I, II A, III B, V

[80] M.I. Shliomis and V.I. Stepanov. Theory of the dynamic susceptibility of magnetic fluids. In William Coffey, editor, *Relaxation Phenomena in Condensed Matter*, volume LXXXVII of *Advances in Chemical Physics*, pages 1–30. John Wiley & Sons, 1994. I, II A, V

[81] Henrik Rogge, Marlitt Erbe, Thorsten M Buzug, and Kerstin Lüdtke-Buzug. Simulation of the magnetization dynamics of diluted ferrofluids in medical applications. *Biomedizinische Technik/Biomedical Engineering*, 58(6):1–9, November 2013. I

[82] Daniel B Reeves and John B Weaver. Combined Néel and Brown rotational Langevin dynamics in magnetic particle imaging, sensing, and therapy. *Applied Physics Letters*, 107(22):223106, December 2015. I

[83] I.S. Poperechny. Combined rotational diffusion of a superparamagnetic particle and its magnetic moment: Solution of the kinetic equation. *J Molec Liq*, 299:112109, 2020. I

[84] Martin Kröger and Patrick Ilg. Combined dynamics of magnetization and particle rotation of a suspended superparamagnetic particle in the presence of an orienting field: Semi-analytical and numerical solution. *Math. Models Meth. Appl. Sci.*, 32(7):1–35, 2022. I, IV A, IV C

[85] Patrick Ilg. Diffusion-jump model for the combined Brownian and Néel relaxation dynamics of ferrofluids in the presence of external fields and flow. *Physical Review E*, 100(2):022608, August 2019. I, II A, II A, II B, II B, III, IV D, V

[86] D. V. Berkov, N. L. Gorn, R. Schmitz, and D. Stock. Langevin dynamic simulations of fast remagnetization processes in ferrofluids with internal magnetic degrees of freedom. *J. Phys.: Condens. Matter*, 18:S2595–S2621, 2006. I, II A, II A, V

[87] C. Haase and U. Nowak. Role of dipole-dipole interactions for hyperthermia heating of magnetic nanoparticle ensembles. *Physical Review B*, 85(4):045435, 2012.

[88] P Ilg and M Kröger. Dynamics of interacting magnetic nanoparticles: effective behavior from competition between Brownian and Néel relaxation. *Phys. Chem. Chem. Phys.*, 22:22244–22259, 2020. I, V, VI, C

[89] Fannin, P.C. and S W Charles. The study of a ferrofluid

exhibiting both Brownian and Neel relaxation. *Journal of Physics D Applied Physics*, 22(1):187–191, January 1989. II A

[90] J.-O. Andersson, C. Djurberg, T. Jonsson, P. Svedlindh, and P. Nordblad. Monte carlo studies of the dynamics of an interacting monodispersive magnetic-particle system. *Phys. Rev. B*, 56(21):13983–13988, 1997. II A

[91] J Carrey, B Mehdaoui, and M Respaud. Simple models for dynamic hysteresis loop calculations of magnetic single-domain nanoparticles: Application to magnetic hyperthermia optimization. *Journal Of Applied Physics*, 109(8):083921, April 2011.

[92] S Ruta, R Chantrell, and O Hovorka. Unified model of hyperthermia via hysteresis heating in systems of interacting magnetic nanoparticles. *Scientific Reports*, 5:9090–7, March 2015.

[93] Christian Jonasson, Vincent Schaller, Lunjie Zeng, Eva Olsson, Cathrine Frandsen, Alejandra Castro, Lars Nilsson, Lara K Bogart, Paul Southern, Quentin A Pankhurst, M Puerto Morales, and Christer Johansson. Modelling the effect of different core sizes and magnetic interactions inside magnetic nanoparticles on hyperthermia performance. *Journal of Magnetism and Magnetic Materials*, 477:198–202, May 2019. II A

[94] D. V. Berkov, N. L. Gorn, and D. Stock. Combined Langevin dynamics/Monte-Carlo simulations of the non-equilibrium ferrofluid remagnetization. *J. Magn. Magn. Mater.*, 272:E1281–E1283, 2004. II A, V

[95] M. A. Martsenyuk, Yu. L. Raikher, and M. I. Shliomis. On the kinetics of magnetization of suspension of ferromagnetic particles. *Sov. Phys. JETP*, 38(2):413–416, 1974. II B, III A, III A, III A

[96] J. T. Waldron, Yu. P. Kalmykov, and W. T. Coffey. Rotational Brownian motion and dielectric relaxation of polar molecules subjected to constant bias field: Exact solution. *Phys. Rev. E*, 49(5):3976–3989, 1994. II B

[97] P. Ilg, M. Kröger, and S. Hess. Magnetoviscosity and orientational order parameters of dilute ferrofluids. *J. Chem. Phys.*, 116(20):9078–9088, 2002. III A, C

[98] B U Felderhof and R B Jones. Nonlinear response of a dipolar system with rotational diffusion to an oscillating field. *J. Phys.: Condens. Matter*, 15(15):S1363–S1378, 2003. III B

[99] Jorge H. Sánchez and Carlos Rinaldi. Magnetoviscosity of dilute magnetic fluids in oscillating and rotating magnetic fields. *Physics of Fluids*, 22(4):043304, 2010. II B

[100] M. Kröger. Simple models for complex nonequilibrium fluids. *Phys. Rep.*, 390(6):453–551, 2004. III, III B

[101] Yu. L. Raikher and M. I. Shliomis. The effective field method in the orientational kinetics of magnetic fluids. *Adv. Chem. Phys.*, 87:595, 1994. III A

[102] P. Ilg, M. Kröger, S. Hess, and A. Yu. Zubarev. Dynamics of colloidal suspensions of ferromagnetic particles in plane Couette flow: Comparison of approximate solutions with Brownian dynamics simulations. *Phys. Rev. E*, 67:061401, 2003. III A, III A

[103] W T Coffey, D S F Crothers, J L Dorman, L J Geoghegan, Yu. P. Kalmykov, J T Waldron, and A W Wickstead. Effect of an oblique magnetic field on the superparamagnetic relaxation time. *Phys. Rev. B*, 52(22):15951, 1995. III A

[104] M. Cobianchi, A. Guerrini, M. Avolio, C. Innocenti, M. Corti, P. Arosio, F. Orsini, C. Sangregorio, and A. Lascialfari. Experimental determination of the frequency and field dependence of specific loss power in magnetic fluid hyperthermia. *Journal of Magnetism and Magnetic Materials*, 444:154–160, 2017. IV D

[105] Nicolas Garraud, Rohan Dhavalikar, Mythreyi Unni, Shehaab Savliwala, Carlos Rinaldi, and David P Arnold. Benchtop magnetic particle relaxometer for detection, characterization and analysis of magnetic nanoparticles. *Physics in Medicine & Biology*, 63(17):175016, 2018. IV E, IV E

[106] Maheshika Palihawadana-Arachchige, Humeshkar Nemala, Vaman M Naik, and Ratna Naik. Effect of magnetic dipolar interactions on temperature dependent magnetic hyperthermia in ferrofluids. *Journal Of Applied Physics*, 121(2):023901, January 2017. V

[107] Patrick Ilg and Martin Kröger. Field- and concentration-dependent relaxation of magnetic nanoparticles and optimality conditions for magnetic fluid hyperthermia. *Scientific Reports*, 13:16523, 2023. V, VI

[108] I M Perreard, D B Reeves, X Zhang, E Kuehlert, E R Forauer, and J B Weaver. Temperature of the magnetic nanoparticle microenvironment: estimation from relaxation times. *Phys. Med. Biol.*, 59(5):1109–1119, 2014. Publisher: IOP Publishing. VI

[109] J C Adams. III. On the expression of the product of any two Legendre's coefficients by means of a series of Legendre's coefficients. *Proceedings Of The Royal Society Of London*, 27(185):63–71, 1878. A

[110] H. C. Öttinger. *Stochastic Processes in Polymeric Fluids*. Springer, Berlin, 1996. C, C